Study of Heat Transfer from a Finned Rotating Cylinder

Jayathi Murthy*
Arizona State University, Tempe, Arizona

Laminar flow and heat transfer from a cylinder with circumferential fins rotating inside a stationary shroud are computed. Centrifugal buoyancy is found to oppose the forced flow and decrease heat-transfer augmentation. The greatest augmentation is found for relatively short fins placed close together. Heat-transfer augmentation is accompanied by an increase in the torque required to rotate the cylinder; this increase is of the same order as the augmentation in heat transfer. Local and overall heat-transfer results are presented as a function of the Taylor and Grashof numbers and geometrical parameters such as the fin clearance and fin spacing.

Nomenclature

C = dimensionless clearance c/d
c = clearance space, Fig. 1
d = distance between cylinder and shroud, Fig. 1
F = dimensionless shear force, Eq. (13)
F_c = value of F for $Ta \to 0$
f = dimensionless shear stress on the shroud surface, Eq. (13)
Gr = rotational Grashof number
k = thermal conductivity of the fluid
$\underline{Nu}$ = local Nusselt number at the shroud surface, Eq. (17)
$\overline{Nu}$ = Nusselt number, Eq. (15)
Nu_c = value of Nu for $Ta \to 0$
P = dimensionless pressure, Eq. (11)
p = pressure
Pr = Prandtl number of the fluid
q = local heat flux at the shroud surface
$\bar{q}$ = average heat flux at the shroud surface
R = radius of the rotating cylinder, Fig. 1
Re = Reynolds number, Eq. (11)
S = dimensionless spacing, s/d
s = spacing between adjacent fins, Fig. 1
T = temperature
T_1 = temperature of the finned cylinder
T_2 = temperature of the shroud
Ta = Taylor number, Eq. (11)
U = dimensionless axial velocity, Eq. (10)
u = axial velocity
V = dimensionless radial velocity, Eq. (10)
v = radial velocity
W = dimensionless circumferential velocity, Eq. (10)
w = circumferential velocity
X = dimensionless axial coordinate, Eq. (9)
x = axial coordinate, Fig. 1
Y = dimensionless radial coordinate, Eq. (9)
y = radial coordinate, Fig. 1
α = thermal diffusivity of the fluid
θ = dimensionless temperature, Eq. (12)
μ = dynamic viscosity of the fluid
ν = kinematic viscosity of the fluid
ρ = density of the fluid
τ = shear stress on the shroud surface
ψ = dimensionless stream function, Eq. (19)
ψ_c = strength of clockwise eddy
ψ_{cc} = strength of counterclockwise eddy
Ω = angular velocity of the rotating cylinder

Received Feb. 9, 1987; revision received Aug. 26, 1987.

*Assistant Professor, Department of Mechanical and Aerospace Engineering.

Introduction

THE operating efficiency of motors and generators may be substantially improved by augmenting the dissipation of internally generated heat to the surroundings. To this end, the surface of the rotor in many rotating machines is provided with grooves, ribs, and other fin-like projections. Fins augment cooling by increasing the surface area available for heat dissipation; more importantly, the presence of fins creates nonuniformities in the flow, setting up secondary vortices. It is this secondary motion that is primarily responsible for improved heat transfer in most practical situations. Therefore, the study of heat transfer from a finned rotating cylinder is relevant to the cooling of electrical machinery.

In the current study, the physical configuration considered is that shown in Fig. 1. Circumferential fins are placed uniformly on a cylinder rotating with a constant angular velocity inside a shroud. The interfin space is filled with a fluid such as air or water. In the absence of density variations, the greater centrifugal force at the rotating fin pushes the fluid outward along the fin, resulting in symmetrical vortices rotating as shown. However, in many practical situations, density gradients due to variations in temperature are significant; in such cases, the denser fluid away from the rotor experiences a centrifugal force greater than that experienced by the less dense fluid near the fin, and a reversal of flow direction may occur. This paper presents a numerical study of the effect of buoyancy due to rotation on heat transfer in the geometry shown. As in most augmentation devices, increased heat transfer due to the presence of fins is invariably accompanied by a penalty in the form of increased frictional drag; consequently, details of the flowfield are also presented.

The only studies in the literature directly related to this geometry are those of Patankar and Murthy[1] and Murthy and Patankar.[2] In the former, forced convection due to rotation is studied, but centrifugal buoyancy ignored. The latter is a study of forced convection with longitudinal fins and

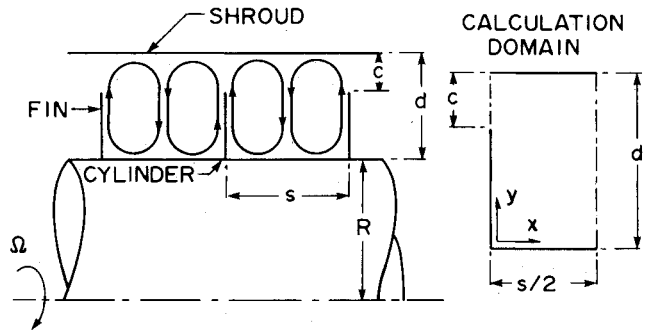

Fig. 1 The physical configuration and the calculation domain.

also ignores centrifugal buoyancy. The present work shares many similarities with augmentation studies in stationary geometries, such as those by Acharya and Patankar[3] and Sparrow et al.;[4] in these studies, the focus is on heat-transfer augmentation with either mixed convection or pure forced convection. Fin geometry plays a central role in augmentation in these situations. Bergeles[5] has presented an extensive review of enhancement techniques using fins. Centrifugal buoyancy effects are important in the study of rotating duct flows, used to model coolant flow in rotor windings. In this type of flow, secondary circulation is created by the nonuniformity of centrifugal and coriolis forces due to the presence of duct walls; in this sense, the situation is similar to that considered in the present work. An extensive review of flow and heat transfer in rotating tubes has been provided by Morris,[6] both for parallel and orthogonal modes. Flow in rotating circular pipes has been studied numerically by Woods and Morris.[7,8] Laminar flow results for square rotating ducts have been provided by Morris and Dias.[9] Neti et al.[10] have computed laminar heat transfer in rectangular channels rotating about a parallel axis. These studies show that the effect of centrifugal buoyancy is significant, especially near the entrance, and acts to change the cellular pattern of secondary flow. The configuration studied in this paper is, of course, somewhat different, both in terms of wall boundary conditions and the direction of rotation; it is an attempt to use fins to dynamically alter the flowfield in order to achieve the augmentation obtained by rotating ducts.

Mathematical Formulation

The steady laminar incompressible flow of a Newtonian fluid in the axisymmetric geometry in Fig. 1 is considered. All properties are deemed constant except the density; the latter is assumed to decrease linearly with temperature through the expansion coefficient β, this variation being manifested only in the centrifugal force. To limit the number of governing parameters, assumptions about the geometry must be made. First, the radius R of the rotating cylinder is assumed to be much larger than d, the clearance between the cylinder and the shroud. Second, the thickness of the fin relative to the interfin spacing is considered small. Both assumptions are reasonable for electrical machinery. As a consequence of the first assumption, the equations governing the flow in the calculation domain (Fig. 1) are reduced to those in Cartesian coordinates, except that a centrifugal force must be included with the attendant variations in density.

The dimensionless equations governing the flow and heat transfer may thus be written as

$$\frac{\partial U}{\partial X} + \frac{\partial V}{\partial Y} = 0 \tag{1}$$

$$U\frac{\partial U}{\partial X} + V\frac{\partial U}{\partial Y} = -\frac{\partial P}{\partial X} + \frac{\partial^2 U}{\partial X^2} + \frac{\partial^2 U}{\partial Y^2} \tag{2}$$

$$U\frac{\partial V}{\partial X} + V\frac{\partial V}{\partial Y} = -\frac{\partial P}{\partial Y} + \frac{\partial^2 V}{\partial X^2} + \frac{\partial^2 V}{\partial Y^2} + Ta^2 W^2 - GrW^2\theta \tag{3}$$

$$U\frac{\partial W}{\partial X} + V\frac{\partial W}{\partial Y} = \frac{\partial^2 W}{\partial X^2} + \frac{\partial^2 W}{\partial Y^2} \tag{4}$$

$$U\frac{\partial \theta}{\partial X} + V\frac{\partial \theta}{\partial Y} = \frac{1}{Pr}\left(\frac{\partial^2 \theta}{\partial X^2} + \frac{\partial^2 \theta}{\partial Y^2}\right) \tag{5}$$

For the calculation domain shown in Fig. 1, the boundary conditions may be written as

Shroud

$$U = 0, \quad V = 0, \quad W = 0, \quad \theta = 0 \tag{6}$$

Cylinder and fin

$$U = 0, \quad V = 0, \quad W = 1, \quad \theta = 1 \tag{7}$$

Other boundaries

$$U = 0 \quad \text{and } \partial/\partial X \quad \text{for } V, W, \theta \tag{8}$$

In the preceding equations, the dimensionless variables have been defined as

$$X = x/d, \quad Y = y/d \tag{9}$$

$$U = ud/\nu, \quad V = vd/\nu, \quad W = w/(R\Omega) \tag{10}$$

$$P = (p/\rho)d^2/\nu^2, \quad Re = R\Omega d/\nu, \quad Ta = Re/(d/R)^{1/2} \tag{11}$$

$$\theta = (T - T_2)/(T_1 - T_2), \quad Pr = \nu/\alpha$$

$$Gr = (R\Omega^2)\,\beta(T_1 - T_2)d^3/\nu^2 \tag{12}$$

The last term in Eq. (3) is a result of the incorporation of density variations in the centrifugal force term. Boundary conditions include the imposition of a constant angular velocity Ω on the cylinder and fins, a no-slip condition at the solid walls, and symmetry conditions elsewhere. For heat transfer, the fins and the cylinder are assumed to be at a uniform temperature T_1 and the shroud at a lower but uniform temperature T_2. These latter assumptions are appropriate for a metallic shroud and cylinder in air. The flow and temperature problems are coupled by the buoyancy term in Eq. (3) and must be solved simultaneously. The flow is governed by the Taylor number Ta, the rotational Grashof number Gr, the Prandtl number Pr, and two geometric quantities, $S\ (= s/d)$ and $C\ (= c/d)$. The magnitudes of Ta and Gr determine the relative importance of forced and buoyant convection.

For purposes of design, it is appropriate to calculate the dimensionless shear force F on the shroud:

$$F = \frac{\int \tau dx}{(\mu R\Omega/d)\int dx} = \frac{\int f dX}{\int dX} \tag{13}$$

where τ is the shear stress on the shroud and x is integrated over the x-direction length of the calculation domain. In terms of the dimensionless variables,

$$F = -(2/S)\int_0^{s/2} (\partial W/\partial Y)\,|_{Y=1} dX \tag{14}$$

Similarly, an overall Nusselt number may be defined:

$$\overline{Nu} = \frac{\bar{q}\,d}{k(T_1 - T_2)} \tag{15}$$

Here, $\bar{q}$ is the average heat flux at the shroud surface. In terms of the dimensionless quantities,

$$\overline{Nu} = -(2/S)\int_0^{s/2} (\partial\theta/\partial Y)\,|_{Y=1} dX \tag{16}$$

In addition, a local Nusselt number Nu may be defined:

$$Nu = \frac{q\,d}{k(T_1 - T_2)} \tag{17}$$

where q is the local heat flux at the shroud. Again,

$$Nu = -\partial\theta/\partial Y\,|_{Y=1} \tag{18}$$

The set of governing equations was solved by the use of the control volume technique described by Patankar.[11] Pressure-velocity coupling was handled using the SIMPLER procedure of Patankar.[12] The results presented in this paper have been obtained for a 28×30 nonuniform grid in the $x - y$ coordinates. Exploratory computations using finer grids indicate that the shear force and the average Nusselt number are accurate to about 3%.

Results and Discussion

The numerical computations yield an overwhelming amount of information about the flow and heat transfer in the

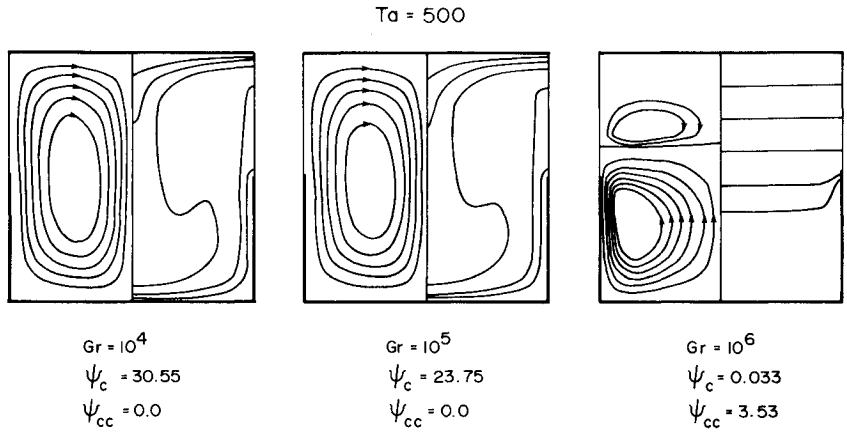

Fig. 2 Contours of the stream function and the temperature for different Grashof numbers for $S = 1.0$, $C = 0.5$, $Pr = 0.7$, $Ta = 500$. Temperature contour levels: 0.2, 0.4, 0.6, 0.8, 0.9.

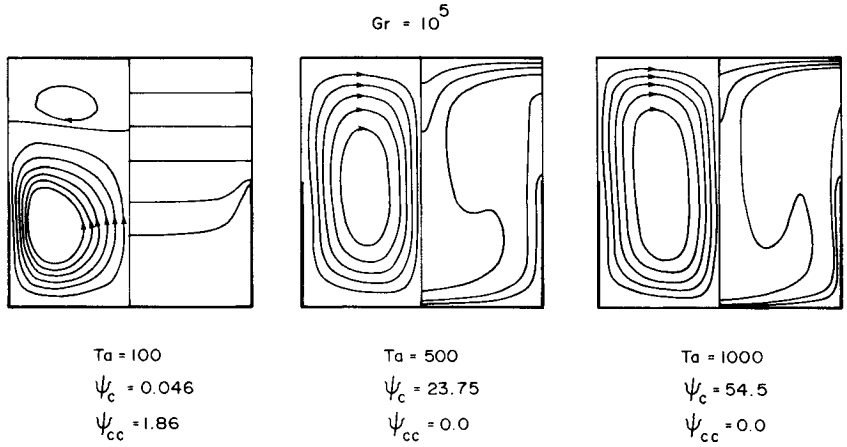

Fig. 3 Contours of the stream function and the temperature for different Taylor numbers for $S = 1.0$, $C = 0.5$, $Pr = 0.7$, $Gr = 10^5$. Temperature contour levels: 0.2, 0.4, 0.6, 0.8, 0.9.

geometry. In the interest of brevity, only selected results will be presented. First, streamline and isotherm patterns will be examined in order to understand the qualitative features of the flow. Then, overall as well as local flow and heat-transfer results will be discussed.

Streamlines and Isotherms

Figures 2 and 3 show plots of the streamlines and isotherms for $S = 1.0$ and $C = 0.5$ as a function of the Taylor and Grashof numbers. Here the streamlines have been plotted on the left half of each diagram and the isotherms on the right half. The domain shown has a width S. The opposing effects of buoyant and forced convection are very clearly in evidence. Pure buoyant convection leads to counterclockwise eddies since the fluid in the interfin space is colder and denser than the fluid near the fin and experiences greater centrifugal force. Pure forced convection, on the other hand, results in clockwise eddies, since the fluid near the fin experiences greater W velocities and hence greater centrifugal force. For mixed convection, some combination of the two opposing tendencies is encountered.

In Fig. 2, the influence of forced convection diminishes as the Grashof number is increased. The quantity ψ_c is a measure of the strength of secondary convection. Here ψ is the dimensionless stream function defined as

$$\psi = -\int_0^Y U\, dY \tag{19}$$

It is seen that the secondary flow loses in strength as the Grashof number is increased. Finally, at a Grashof number of 10^6, the interfin space is filled with a weak counterclockwise eddy driven by buoyant convection. Significant distortion of isotherms is found when forced convection effects are dominant, as at $Gr = 10^4$ and $Gr = 10^5$. Thin thermal boundary layers are evident on the shroud over the fin due to the impingement of heated fluid. Distortion of isotherms is minimal when buoyant convection is primarily responsible for the secondary flow, as at $Gr = 10^6$. Similar effects are to be found in Fig. 3. It is evident that any augmentation in heat transfer must be the result of forced convection; secondary motion due to pure buoyant convection is extremely weak, and acts primarily to retard the forced flow.

Results for Vanishing Taylor and Grashof Numbers

For vanishing values of the Taylor number, buoyant convection is primarily responsible for the secondary motion. The values of the shear force on the shroud and the overall Nusselt number so obtained are denoted by F_c and $\overline{Nu}_c$, respectively. These limiting values are a function of the geometry as well as the Grashof and Prandtl numbers. For the case when both the Taylor and Grashof numbers tend to zero, the effect of the centrifugal forces in inducing secondary motion is negligibly small. In the absence of secondary motion, both W and θ satisfy the Laplace equation and identical boundary conditions. In this limit, it follows that F_c is equal to $\overline{Nu}_c$ and that both F_c and $\overline{Nu}_c$ are functions of the geometry alone. These values are the "conduction limit" to the problem and represent the minimum possible shear force and heat transfer possible in this geometry.

Table 1 Values of F_c and $\overline{Nu}_c$ for $Pr = 0.7$

Geometry	$Gr = 0$		$Gr = 10^3$		$Gr = 10^4$		$Gr = 10^5$		$Gr = 10^6$	
	F_c	$\overline{Nu}_c$	F_c	$\overline{Nu}_c$	F_c	$\overline{Nu}_c$	F_c	$\overline{Nu}_c$	F_c	$\overline{Nu}_c$
$S=2$, $C=0.0$	3.61	3.61	3.63	3.62	3.84	3.73	4.34	4.03	5.30	4.66
$S=2$, $C=0.5$	1.2	1.2	1.22	1.21	1.29	1.25	1.37	1.30	1.47	1.38
$S=1$, $C=0.0$	6.66	6.66	6.66	6.66	6.83	6.74	7.38	7.06	8.53	7.79
$S=1$, $C=0.5$	1.39	1.39	1.40	1.40	1.45	1.42	1.52	1.47	1.60	1.52
$S=0.5$, $C=0.0$	11.09	11.09	11.09	11.09	11.09	11.09	11.46	11.26	12.71	11.98
$S=0.5$, $C=0.5$	1.62	1.62	1.62	1.62	1.62	1.62	1.66	1.64	1.71	1.67

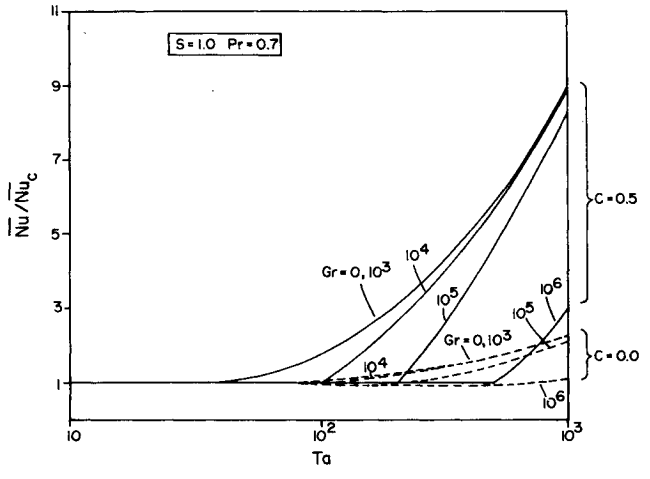

Fig. 4 Variation of overall heat transfer with Taylor number for $S = 1.0$, $Pr = 0.7$.

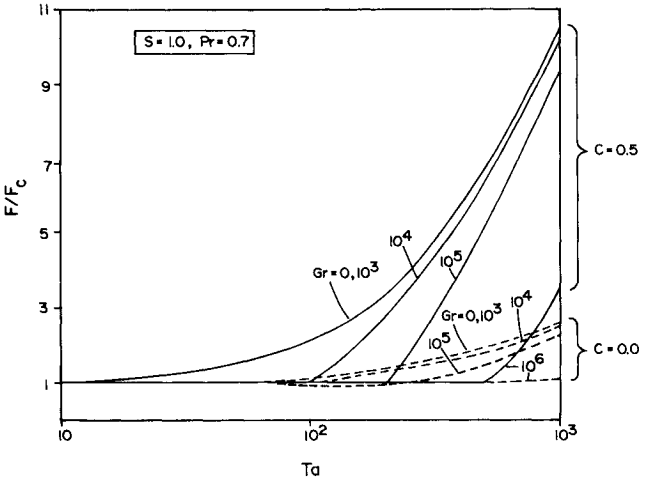

Fig. 6 Variation of shear force on the shroud with Taylor number for $S = 1.0$, $Pr = 0.7$.

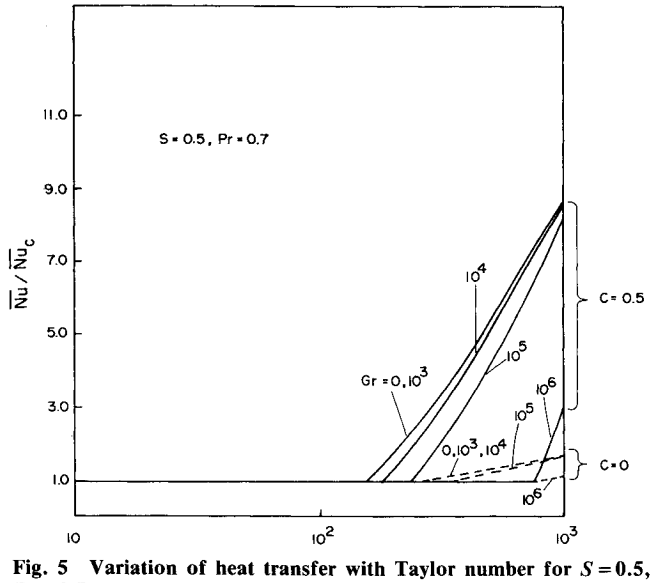

Fig. 5 Variation of heat transfer with Taylor number for $S = 0.5$, $Pr = 0.7$.

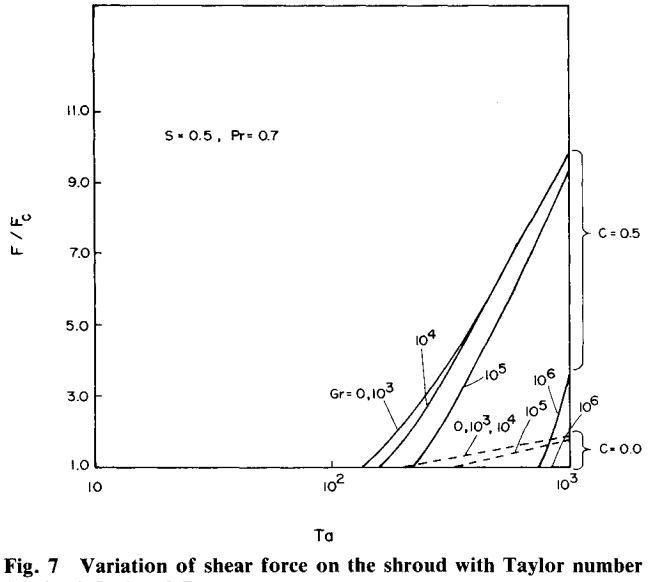

Fig. 7 Variation of shear force on the shroud with Taylor number for $S = 0.5$, $Pr = 0.7$.

All overall results presented in this paper are referenced to F_c and $\overline{Nu}_c$ for the Grashof number under consideration. Table 1 lists F_c and $\overline{Nu}_c$ for the various governing parameters for $Pr = 0.7$. The values of F_c for $Gr = 0$ are identical to those presented in Ref. 1. It may be seen that only minimal augmentation over the conduction limit may be obtained for pure buoyant convection.

Overall Nusselt Number and Shear Force

The ratio $\overline{Nu}/\overline{Nu}_c$ is plotted vs the Taylor number in Figs. 4 and 5. The corresponding variations of F/F_c are plotted in Figs. 6 and 7. Each figure has been drawn for a particular value of the interfin spacing S and two values of the clearance parameter C. The Prandtl number is held constant at 0.7.

Secondary motion enhances heat transfer by as much as nine times; the increase in the shear force is somewhat higher. For $Ta \to 0$, the flow is dominated by centrifugally driven buoyant convection. In this limit, Table 1 shows that the higher Grashof numbers lead to the greater heat transfer and shear force. As the Taylor number is increased, forced convection plays an increasingly important role and becomes the dominant effect as $Ta \to \infty$. Curves for various Grashof

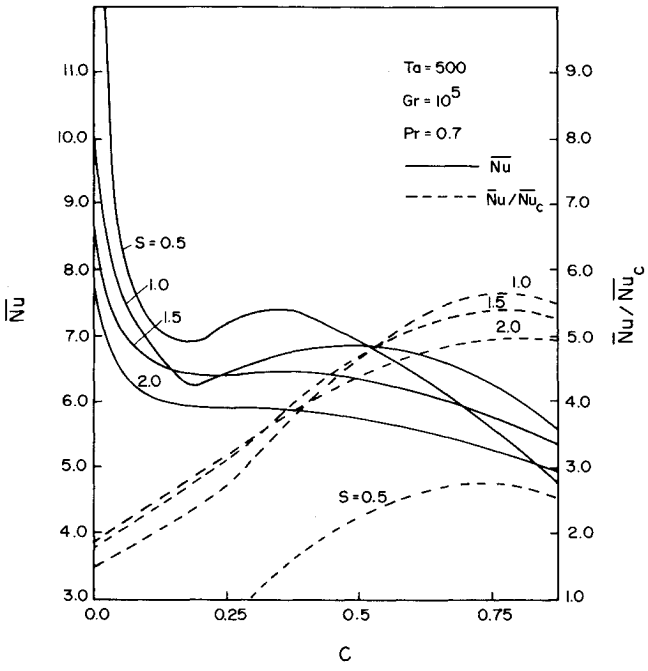

Fig. 8 Effect of geometry on the overall Nusselt number.

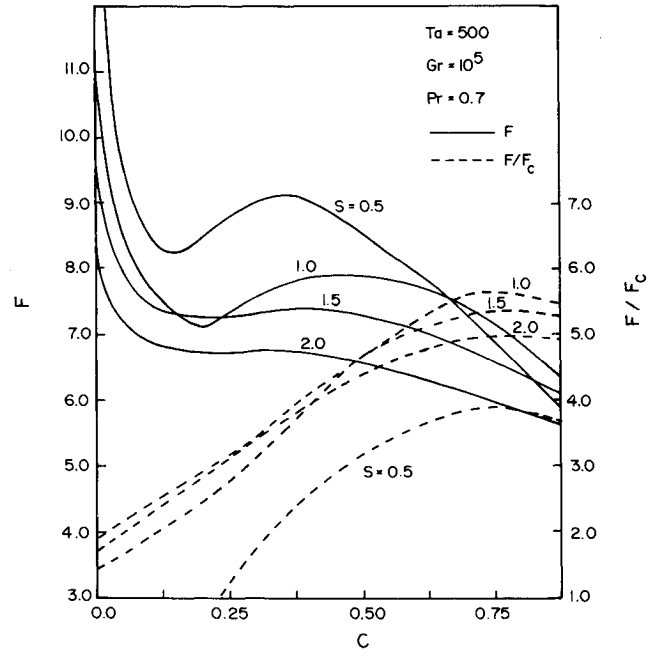

Fig. 9 Effect of geometry on the overall shear force.

numbers merge together and approach the forced convection limit in Ref. 1. As expected, flows with lower Grashof numbers give way more readily to forced convection than do those with higher Grashof numbers.

Effect of Geometry

Fin geometry plays an important role in heat-transfer augmentation. This is amply borne out by the variation of the shear force and overall Nusselt number with the fin clearance parameter C in Figs. 8 and 9.

The dominant flow pattern is that of a single eddy rotating clockwise; for shorter fins, the flow gives way to a two-eddy pattern for $S > 2.0$. Flow in the long-fin geometries is strongly retarded by friction. The value of ψ_c for $S = 1.0$, $C = 0.0$ is 22.9, whereas that for $S = 1.0$, $C = 0.5$ is 23.7. Thus, flow in the long-fin geometries is strongly retarded by friction, despite

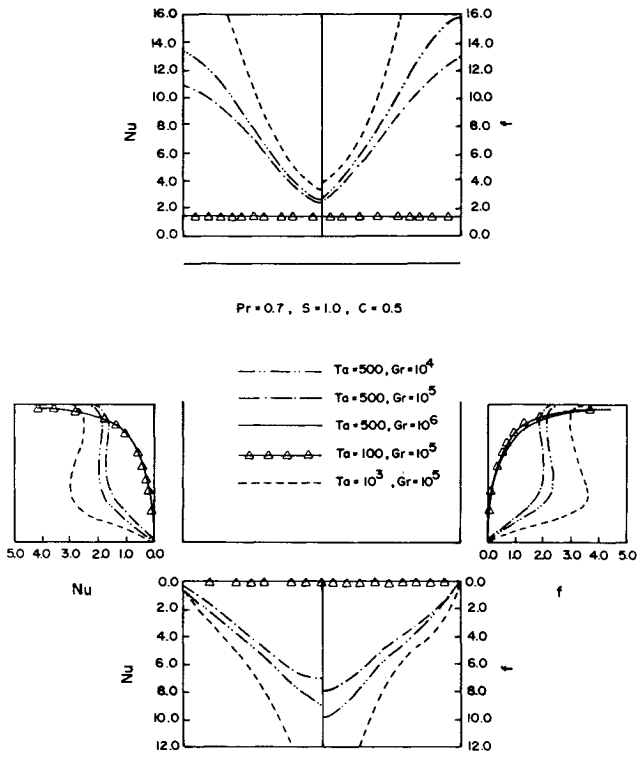

Fig. 10 Local heat-transfer and shear stress variation.

the greater input of angular momentum associated with long fins. Frictional retardation ceases to be a significant factor for large fin spacing; the value of ψ_c decreases from 36.7 to 31.5 as C changes from 0.0 to 0.5 for a fin spacing of $S = 2.0$.

In Figs. 8 and 9, the highest heat transfer and shear force are to be found for vanishing fin clearance, as the gradients of azimuthal velocity and temperature become exceedingly large at the fin tip. In the absence of fins, F and $\overline{Nu}$ both tend to unity. The intermediate variation depends on fin spacing. For closely spaced fins, two opposing effects come into play. As the fin length decreases, F and $\overline{Nu}$ tend to decrease as the gradients of W and θ decrease at the fin tip. On the other hand, increased vortex strength for short fins tends to increase both F and $\overline{Nu}$. Thus, a local maximum in F and $\overline{Nu}$ is found at approximately $C = 0.5$ in Figs. 8 and 9 for $S = 0.5$ and $S = 1.0$. For fins spaced far apart, vortex strength decreases with an increase in C; thus, F and $\overline{Nu}$ decrease monotonically with C for $S = 2.0$.

The greatest augmentation in heat transfer and shear force occurs for short fins, as seen in the curves for $\overline{Nu}/\overline{Nu}_c$ and F/F_c in Figs. 8 and 9. The secondary flow, rotating in a clockwise direction, transports the cooler fluid from the shroud to the cylinder. An examination of the isotherms in Figs. 2 and 3 reveals that the greatest heat transfer occurs at the point of impingement; thereafter, the thermal boundary layer thickens and the rate of heat transfer decreases. This is borne out by the local heat-transfer behavior described in the next section. A similar argument can be made regarding the shear force.

The trend with respect to interfin spacing depends on the fin clearance. Short fins do no impart enough angular momentum to the fluid to drive a wide cavity; consequently, the greatest augmentation takes place when they are placed close together. Long fins, however, are able to drive a wider cavity and can take advantage of an increase in S. Thus, the greatest augmentation for long fins occurs when they are placed far apart. When the fin spacing becomes very small, as in the case of $S = 0.5$, frictional retardation is so great that even short fins do not provide adequate augmentation; thus, the augmentation curve for $S = 0.5$ falls below all others in Figs. 8 and 9.

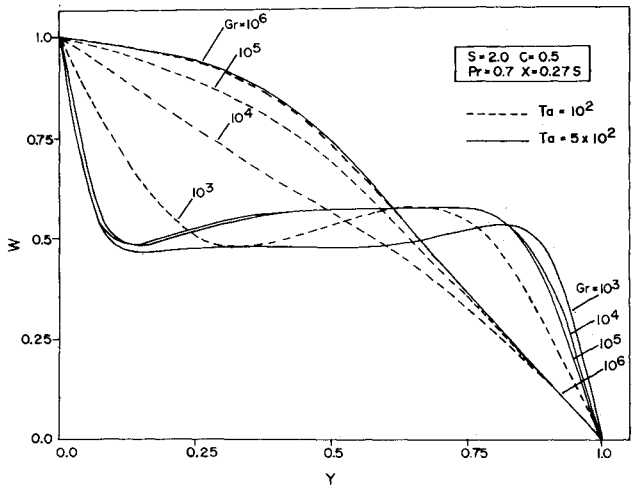

Fig. 11 Variation of circumferential velocity.

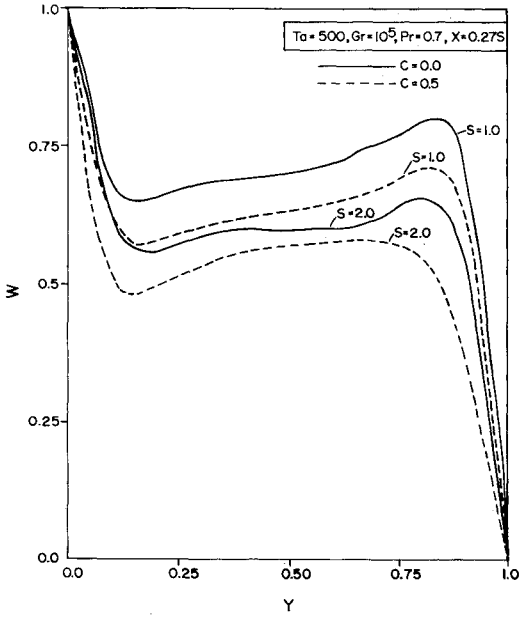

Fig. 12 Variation of circumferential velocity with geometry.

Local Nusselt Number and Shear Stress

The nonuniformity of the local Nusselt number and the dimensionless shear stress f is a measure of the strength of the secondary convection, as seen in Fig. 10. Here the variation of the local Nusselt number is plotted on the left half of the diagram and that of the shear stress on the right half. On the shroud, the maximum heat transfer and shear stress occur above the fin because of the proximity of fin and shroud and the resulting maximization of θ and W gradients. On the cylinder, the maximum heat transfer and shear stress occur at the point of impingement and decrease toward the base of the fin as both thermal and hydrodynamic boundary layers grow. The heat transfer on the fin exhibits a maximum at the point of impingement of the turning flow; there is another region of high heat transfer at the fin tip. In between, a minimum in heat transfer is seen; it is this minimum that decreases the effectiveness of long fins. The base of the fin is largely insulated from the flow and does not contribute actively to either the heat transfer or the overall torque. The retardation of secondary motion at high Grashof numbers is clearly evident; for $Gr = 10^6$, $Ta = 500$, the Nusselt number and shear stress distributions on the shroud are uniform, and there is virtually no heat transfer or shear stress on the cylinder. The same is true for low Taylor numbers.

The remarkable similarity of the θ and W fields is, of course, a direct consequence of the similarity in governing equations [Eqs. (4) and (5)] and boundary conditions [Eqs. (6-8)]; the small differences are a result of the Prandtl number being 0.7, not unity.

Profiles of Circumferential Velocity

The variation of the circumferential velocity in the calculation domain is shown in Figs. 11 and 12. In these graphs, W is plotted vs the coordinate Y for a location $X = 0.27S$.

W profiles for high Grashof numbers exhibit little distortion due to secondary motions. However, as the Grashof number decreases (or as the Taylor number increases), the distortion becomes increasingly pronounced. The local minimum near the cylinder and the local maximum near the shroud are due to the convection of low-W fluid from the shroud to the cylinder in the former case and the convection of high-W fluid from the cylinder to the shroud in the latter case. No striking changes in the W profiles are to be found as the interfin spacing is changed or as the fin clearance is increased.

Conclusion

Centrifugally driven buoyant convection serves primarily to retard forced convection in the geometry considered and decreases heat-transfer augmentation. The effect is significant for high values of the Grashof number and disappears for high Taylor numbers. Heat-transfer augmentation is particularly sensitive to geometry. The most important result appears to be that the greater heat-transfer augmentation is to be obtained with short fins placed relatively close together.

A re-examination of some of the assumptions made in this paper is in order. The assumption of an isothermal fin can be realized only if the thermal conductivity of the fin is high compared to that of the fluid, as in the case of metallic fins. Fin thickness may also not be negligible. In this event, a conjugate heat-transfer problem must be solved to obtain the fin temperature distribution. Computational procedures for such problems have been outlined by Patankar[11] and are a simple extension of the procedures employed here. A non-isothermal fin would lead to a loss in heat-transfer performance as temperature gradients at the fin surface would decrease. On the other hand, the opposing effects of buoyant convection would be minimized as lateral temperature gradients became smaller. A fin of finite thickness would isolate the region above the tip from the recirculating flow, shifting the local maximum in shroud heat transfer toward the center of the cavity.

The maximum Taylor number in this study has been kept relatively low so as to justify the assumption of laminar flow. No guidelines are available in the literature to predict the onset of turbulence in this specific geometry. The flow due to a disk rotating in a housing becomes turbulent for a Reynolds number, based on a disk radius of 3×10^5, according to Schlichting.[13] This is approximately the maximum value investigated here if d/R is about 0.1. Perhaps a more pertinent configuration is that of a Taylor vortex flow, which remains laminar until a Taylor number of about 1700 for $d/R = 0.2$, also according to Schlichting.[13] The computation of turbulent flow in this geometry is complicated considerably by the presence of body forces and streamline curvature; it remains to be seen whether standard models of turbulence such as the $k - \epsilon$ model will produce useful local predictions. The present study may, however, be used for general understanding of heat-transfer behavior.

References

[1]Patankar, S. V. and Murthy, J. Y., "Analysis of Heat Transfer from a Rotating Cylinder with Circumferential Fins," Symposium on Heat and Mass Transfer in Rotating Machinery, Dubrovnik, Yugoslavia, Aug. 30, 1982.

[2]Murthy, J. Y. and Patankar, S. V., "A Numerical Study of Heat Transfer from a Rotating Cylinder with External Longitudinal Fins,"

Numerical Heat Transfer, Vol. 6, 1983, pp. 463–473.

[3]Acharya, S. and Patankar, S. V., "Laminar Mixed Convection in a Shrouded Fin Array," *Journal of Heat Transfer,* Vol. 103, 1981, pp. 559–565.

[4]Sparrow, E. M., Baliga, B. R., and Patankar, S. V., "Forced Convection Heat Transfer from a Shrouded Fin Array with and without Tip Clearance," *Journal of Heat Transfer,* Vol. 100, 1978, pp. 572–579.

[5]Bergeles, A. E., "Survey and Evaluation of Techniques to Augment Convective Heat and Mass Transfer," *Progress in Heat and Mass Transfer,* Vol. 1, Pergamon Press, Oxford, 1969, pp. 331–424.

[6]Morris, W. D., *Heat Transfer and Fluid Flow in Rotating Coolant Channels,* Research Studies Press, 1981.

[7]Woods, J. L. and Morris, W. D., "An Investigation of a Laminar Flow in the Rotor Windings of Directly-Cooled Electrical Machines," *Journal of Mechanical Engineering Science,* Vol. 16, 1974, pp. 408–417.

[8]Woods, J. L. and Morris, W. D., "A Study of Heat Transfer in a Rotating Cylindrical Tube," *Journal of Heat Transfer,* Vol. 102, 1980, pp. 612–621.

[9]Morris, W. D. and Dias, F. M., "Laminar Heat Transfer in Square Sectioned Ducts which Operate in Rotate in a Parallel Mode," *Power Industry Research,* Vol. 1, 1981.

[10]Neti, S., Warnock, A. S., Levy, E. K., and Kannan, K. S., "Computation of Laminar Heat Transfer in Rotating Rectangular Ducts," *Journal of Heat Transfer,* Vol. 107, 1985, pp. 575–582.

[11]Patankar, S. V., *Numerical Heat Transfer and Fluid Flow,* McGraw-Hill, Hemisphere, New York, 1980.

[12]Patankar, S. V., "A Calculation Procedure for Two-Dimensional Elliptic Situations," *Numerical Heat Transfer,* Vol. 4, 1981, pp. 409–425.

[13]Schlichting, H., *Boundary Layer Theory,* McGraw-Hill, New York, 1979.